PROCEEDINGS OF SPIE

SPIEDigitalLibrary.org/conference-proceedings-of-spie

Image quality of data products of the high resolution telescope of the polarimetric and helioseismic imager

F. Kahil, A. Gandorfer, J. Hirzberger, D. Orozco Suárez, K. Albert, et al.

F. Kahil, A. Gandorfer, J. Hirzberger, D. Orozco Suárez, K. Albert, N. Albelo Jorge, T. Appourchaux, A. Álvarez-Herrero, J. Blanco Rodríguez, D. Germerott, L. Guerrero, P. Gutierrez Marquez, J. Sinjan, D. Calchetti, M. Kolleck, S. K. Solanki, J. C. del Toro Iniesta, R. Volkmer, J. Woch, B. Fiethe, J. M. Gómez Cama, I. Pérez-Grande, E. Sanchis Kilders, M. Balaguer Jiménez, L. R. Bellot Rubio, M. Carmona, W. Deutsch, G. Fernandez-Rico, A. Fernández-Medina, P. García Parejo, J. L. Gasent Blesa, L. Gizon, B. Grauf, K. Heerlein, A. Korpi-Lagg, T. Lange, A. López Jiménez, T. Maue, R. Meller, H. Michalik, A. Moreno Vacas, R. Müller, E. Nakai, W. Schmidt, J. Schou, U. Schühle, J. Staub, H. Strecker, I. Torralbo, G. Valori, "Image quality of data products of the high resolution telescope of the polarimetric and helioseismic imager," Proc. SPIE 12180, Space Telescopes and Instrumentation 2022: Optical, Infrared, and Millimeter Wave, 121803F (27 August 2022); doi: 10.1117/12.2628942

SPIE.

Event: SPIE Astronomical Telescopes + Instrumentation, 2022, Montréal, Québec, Canada

Image Quality of Data Products of the High Resolution Telescope of the Polarimetric and Helioseismic Imager

F. Kahil[1], A. Gandorfer[1], J. Hirzberger[1], D. Orozco Suárez[2], K. Albert[1], N. Albelo Jorge[1], T. Appourchaux[3], A. Alvarez-Herrero[4], J. Blanco Rodríguez[5], D. Germerott[1], L. Guerrero[1], P. Gutierrez Marquez[1], J. Sinjan[1], D. Calchetti[1], M. Kolleck[1], S.K. Solanki[1], J.C. del Toro Iniesta[1], R. Volkmer[6], J. Woch[1], B. Fiethe[7], J.M. Gómez Cama[8], I. Pérez-Grande[9], E. Sanchis Kilders[5], M. Balaguer Jiménez[2], L.R. Bellot Rubio[2], M. Carmona[8], W. Deutsch[1], G. Fernandez-Rico[1,9], A. Fernández-Medina[4], P. García Parejo[4], J.L. Gasent Blesa[5], L. Gizon[1,11], B. Grauf[1], K. Heerlein[1], A. Korpi-Lagg[1], T. Lange[7], A. López Jiménez[2], T. Maue[6], R. Meller[1], H. Michalik[7], A. Moreno Vacas[2], R. Müller[1], E. Nakai[6], W. Schmidt[6], J. Schou[1], U. Schühle[1], J. Staub[1], H. Strecker[2], I. Torralbo[9], and G. Valori[1]

[1]Max-Planck-Institut für Sonnensystemforschung, Justus-von-Liebig-Weg 3, 37077 Göttingen, Germany

[2] Instituto de Astrofísica de Andalucía (IAA-CSIC), Apartado de Correos 3004, E-18080 Granada, Spain

[3] Univ. Paris-Saclay, Institut d'Astrophysique Spatiale, UMR 8617, CNRS, Bâtiment 121, 91405 Orsay Cedex, France

[4]Instituto Nacional de Técnica Aeroespacial, Carretera de Ajalvir, km 4, E-28850 Torrejón de Ardoz, Spain

[5]Universitat de València, Catedrático José Beltrán 2, E-46980, Paterna-Valencia, Spain

[6]Leibniz-Institut für Sonnenphysik, Schöneckstr. 6, D-79104, Freiburg, Germany

[7]Institut für Datentechnik und Kommunikationsnetze der TU Braunschweig, Hans-Sommer-Str. 66, 38106 Braunschweig, Germany

[8]University of Barcelona, Department of Electronics, Carrer de Martíi Franquès, 1 - 11, 08028 Barcelona, Spain

[9]Instituto Universitario "Ignacio da Riva", Universidad Politécnica de Madrid, IDR/UPM, Plaza Cardenal Cisneros 3, E-28040 Madrid, Spain

[11]Institut für Astrophysik, Georg-August-Universität Göttingen, Friedrich-Hund-Platz 1, 37077 Göttingen, Germany

Further author information: (Send correspondence to Fatima Kahil)
E-mail: kahil@mps.mpg.de

Space Telescopes and Instrumentation 2022: Optical, Infrared, and Millimeter Wave, edited by Laura E. Coyle, Shuji Matsuura, Marshall D. Perrin, Proc. of SPIE Vol. 12180, 121803F · © 2022 SPIE · 0277-786X · doi: 10.1117/12.2628942

ABSTRACT

The High Resolution Telescope (HRT) of the Polarimetric and Helioseismic Imager (SO/PHI) on-board the Solar Orbiter mission (SO) provides near diffraction limited observations of the solar surface. The HRT Refocus Mechanism (HRM) allows for acquiring calibration data in flight which are used in post processing on ground to estimate the image quality of SO/PHI-HRT data products and its dependence on the SO-Sun distance. Our aim is to characterise the wavefront aberrations in the optical path of SO/PHI-HRT and consequently the image quality in the focal plane of the telescope. We use calibration data taken during the Near Earth Commissionning Phase (NECP) and the second Remote Sensing Check-out Window (RSCW2) of Solar Orbiter's Cruise Phase (CP). In particular, we apply a Phase Diversity (PD) analysis to estimate the low-order wavefront aberrations. The restoration with the retrieved Point Spread Function (PSF) from the PD analysis increases the RMS contrast of the solar granulation in the visible continuum from 4 % to 10−11 %.

Keywords: Solar Orbiter, SO/PHI, SO/PHI-HRT, high resolution, PSF, Zernike, MTF, wavefront error

1. INTRODUCTION

The Solar Orbiter (SO) mission[1] was launched from Cape Canaveral on February 10, 2020. The six remote sensing (RS) instruments of SO observe the different layers of the solar atmosphere while the four in-situ instruments characterise the solar environment. The Polarimetric and Helioseismic Imager (SO/PHI)[2] is one of the RS instruments, and provides continuum, line-of-sight (LOS) velocity and magnetic field vector maps of the solar surface. Those physical quantities are either obtained by autonomous on-board processing of the raw data[3] or by post processing on ground. The two telescope channels of SO/PHI map the solar scene at high resolution with its High Resolution Telescope (SO/PHI-HRT)[4] or in full-disc mode with the Full Disc Telescope (SO/PHI-FDT).

The data presented in this work are acquired by SO/PHI-HRT during the Near Earth Commissioning Phase (NECP) which started in February, 2020 and during the second Remote Sensing Checkout Window (RSCW2) of the Cruise Phase (CP), which started in June, 2020. For more information on the observing planning strategy for the various instruments on-board the Solar Orbiter spacecraft we recommend the reader to check Zouganelis et al.(2020).[5] During NECP and CP, the RS instruments are switched on to calibrate and characterise the instruments to be ready for the Nominal Mission Phase (NMP), which started late December, 2021.

Characterising the image quality of SO/PHI data products and retrieving the Point Spread Function (PSF) of the optical system are two of the main objectives of the calibration campaigns during CP. SO/PHI-HRT is equipped with a Refocus Mechanism (HRM)[2] that allows for taking focus series of images suitable for a Phase Diversity (PD) wavefront sensing analysis on ground.[6–8] The low-order wavefront aberrations, captured by the PD technique, are responsible for a severe drop in contrast in observations of the solar surface, as demonstrated in.[9] A PD image pair consists of a focused image that has been degraded by the unknown aberrations, and another image which is manually defocused by a certain well defined value, in addition to being affected by the unknown aberrations. To characterise the wavefront error, we use Zernike Polynomials[10,11] which are then built into the PSF of the telescope by autocorrelation of the complex pupil function of the telescope.[12–14] The PSF is then used to restore the observed scene. To characterise the image quality, the normalized Root Mean Square (RMS) contrast of the solar granulation intensity in the continuum wavelength is computed. This quantity is often used in image quality assessment of solar telescopes.[15,16] In Section 2, we present the PD data, describe the PD fitting algorithm, and show the results of wavefront fitting and image restoration.

2. PHASE DIVERSITY ANALYSIS

The data used for the PD analysis consist of the PD image pairs of a quiet-Sun region taken with the Flight Model (FM) of SO/PHI during the NECP on April 20, 2020 (PHI-5) and during RSCW2 on February 20, 2021 (STP-136) at SO-Sun distances of 0.82 AU and 0.52 AU, respectively.

The artificial defocus introduced to the focused images is equal to half of the SO/PHI-HRT wavelength ($\lambda/2$). The defocusing is done by moving the magnifying lenses which are a part of the HRM. The data are first calibrated; this includes dark subtraction and flat-fielding. The focused and defocused images are not obtained simultaneously, so the latter is aligned by cross correlation to sub-pixel accuracy to the former. By

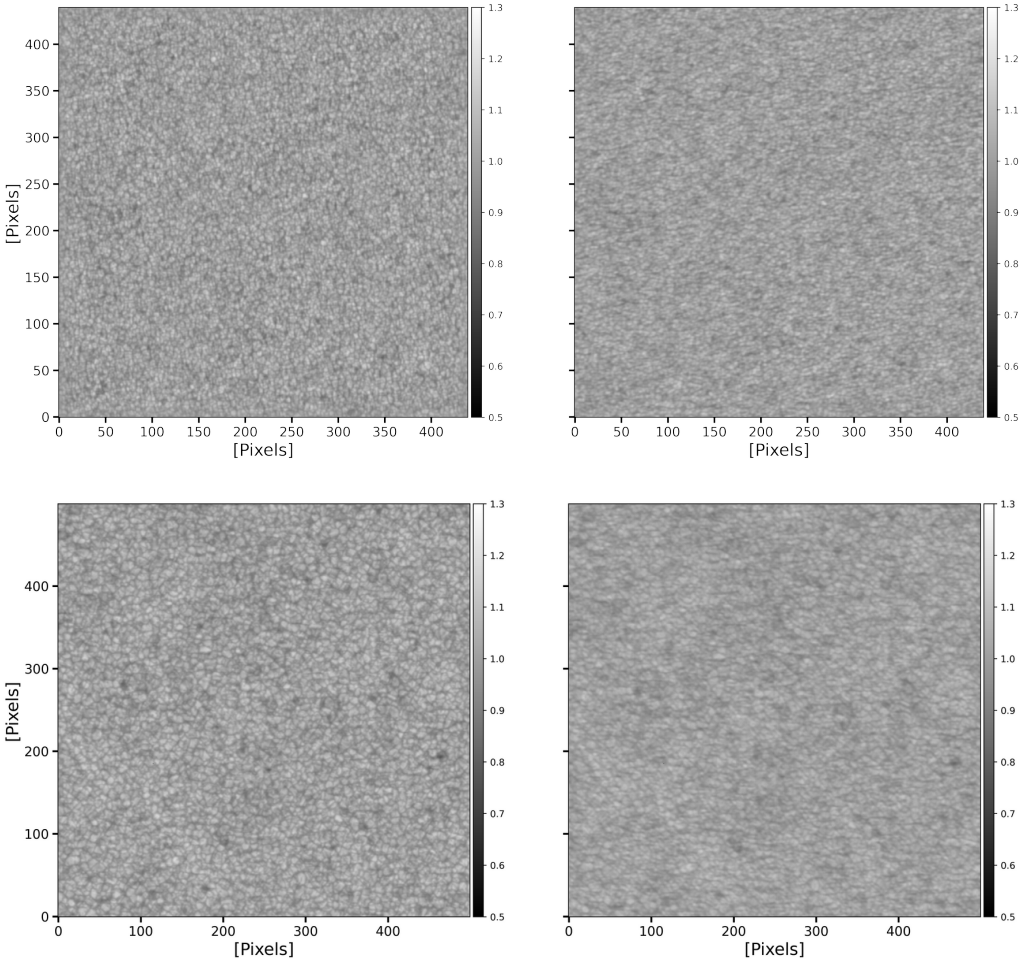

Figure 1. Focused (left column) and defocused (right column) images of a quiet Sun region in the continuum during NECP on April 20, 2020 at a distance of 0.82 AU (top row) and during RSCW2 on February 20, 2021 at a distance of 0.523 AU (bottom row). Each image corresponds to the central sub-region (500×500 pixels) of the obtained data of initial size of 2048×2048 pixels.

doing so, we avoid systematic errors in the fitted wavefront. The PD analysis is applied to images in Fourier space, so we apodize the edges of the data using a cosine function with an edge rim that corresponds to 10 % of the total size of the image. The geometrical shifts for SO/PHI-HRT are listed in Table 1 for all employed data.

Date	Solar distance	Name	$(\Delta x, \Delta y)$ [pixels]	RMS WFE [λ]
20-04-2020	0.82 AU	PHI-5	(3.212, -7.955)	1/10
20-02-2021	0.523 AU	STP-136	(3.326,-8.36)	1/7

Table 1. Summary of phase diversity data. *First column:* The acquisition dates of the PD image pairs. *Second column:* The distance from the Sun. *Third column:* Name of the mission phase during which the PD data are acquired. *Forth column:* Pixel shifts of the defocused image with respect to the focused image. *Fifth column:* The total RMS wavefront error.

2.1 Algorithm and code implementation

We refer to the PD algorithm presented in[7] and develop an open source Python phase-diversity code *. The code minimizes the so-called Error Metric, which returns the difference between the observed image and an estimated image. The latter is the convolution of an estimated initial scene (without aberrations) with an estimated Optical Transfer Function (OTF). The code iterates over the Zernike Polynomials[10] and constructs the OTF used in the minimization process. To avoid fitting the noise in the process of minimizing the error metric, a cutoff noise filter is used where frequencies above a certain threshold are excluded from the fitting process. This cutoff corresponds to the spatial resolution of the SO/PHI-HRT (of 1.0″).

To reduce computational time and test for the dependence of the wavefront error on the field of view of SO/PHI-HRT, the PD code is run on small sub-regions (256×256 pixels each) of the PD image pair. In the process of fitting the wavefront, we start with the first order aberrations. We then increase the number of coefficients as free parameters and check for the overall shape of the fitted wavefront and the restored scene by image deconvolution. We found that the first 10 Zernike coefficients are enough to capture the wavefront error. The piston and tip/tilt coefficients are negligible, so we disregard them as free parameters and consider only the following 10 aberrations: the first order aberrations including the defocus, 0° and 45° astigmatism, x/y coma, and x/y trefoil, in addition to spherical aberration and second order 0° and 45° astigmatism.

Another advantage of using a limited number of Zernike parameters is to reduce the noise amplification during the restoration process. This was demonstrated by Hirzberger et al. (2011)[17] who found increased noise levels and over-reconstruction of synthetic images if larger numbers of Zernike polynomials are used in the PD fitting algorithm.

2.2 Wavefront fitting results

In Figure 2 we show the computed wavefront errors in 36 sub-regions of dimensions of 256×256 pixels each, along with the corresponding Modulation Transfer Functions (MTFs) as deduced from the analysis of PD image pairs taken at 0.8 AU (top row) and at a distance of 0.5 AU (bottom row).

The Zernike coefficients returned by the PD algorithm for each image pair and averaged over the subregions of the whole Field of View (FOV) are shown in Figure 3. During PHI-5 (at 0.8 AU) the main contributors to the wavefront error is astigmatism. The Zernike terms during STP-136 (0.5 AU) which are higher compared to PHI-5 are the spherical aberration and trefoil. These terms are expected to increase closer to the Sun under hotter operational conditions present there, which affect mainly the Heat Rejection Entrance Window (HREW).

For a quantitative assessment of the wavefront error, the total RMS wavefront error is computed. This is simply the square root of the summation of the powered Zernike coefficients, following Noll's expansion scheme of orthonormal polynomials.[10] The values are listed in the last column of Table 1. The wavefront error increases from $\lambda/10$ at 0.82 AU to $\lambda/7$ at 0.523 AU due to the amplification of the individual Zernike terms.

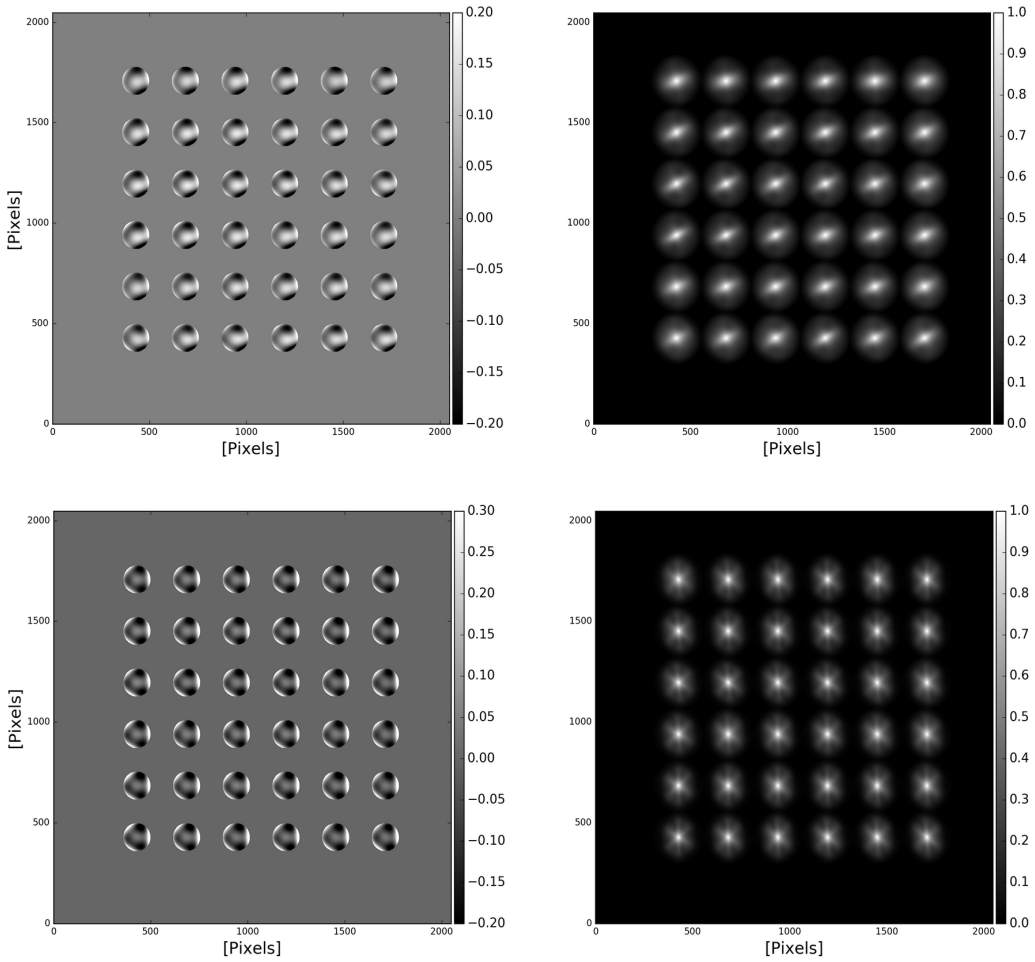

Figure 2. The wavefront error (left column) and MTF (right column) distribution across the full SO/PHI-HRT FOV. Each row corresponds to the PD image pair taken during PHI-5 at 0.8 AU (top row) and STP-136 at 0.523 AU (bottom row). The PD code is run on sub-regions of 256×256 pixels each.

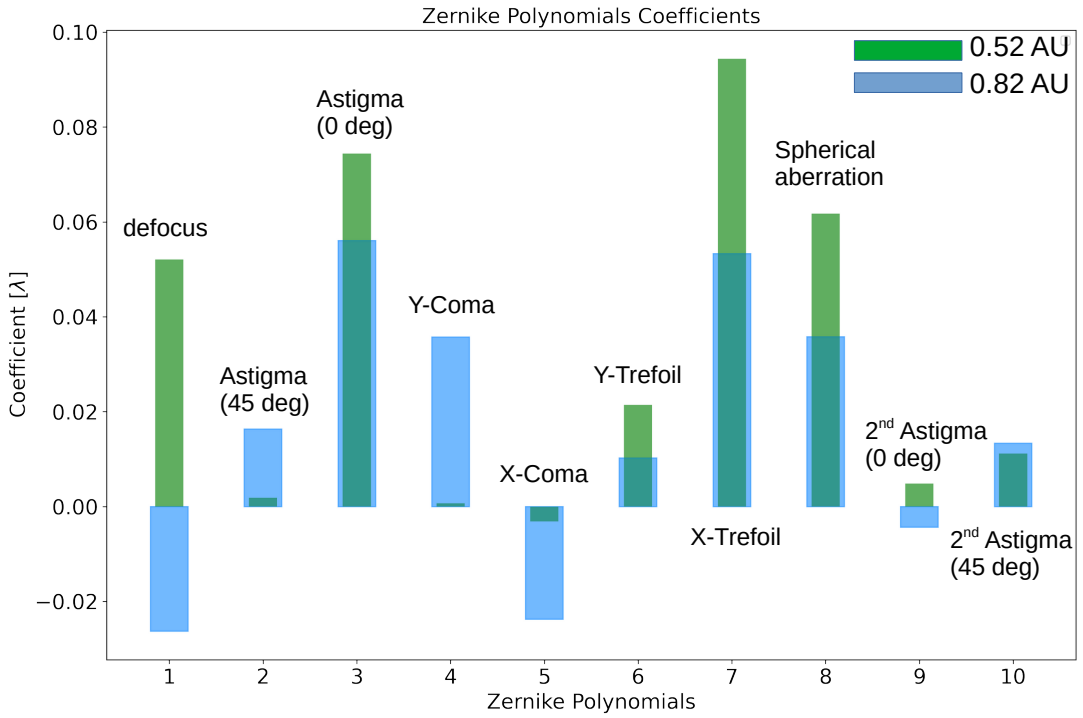

Figure 3. The Zernike coefficients in units of wavelength deduced from the analysis of the PD image pair of the QS granulation at 0.5 AU and at 0.8 AU. The name of the wavefront aberration of each Zernike term is written above/below the corresponding bars.

2.3 Data Restoration

We compute the averaged PSF over the FOV by a Fourier transform applied on the averaged MTFs. Then we restore images of quiet-Sun granulation by image deconvolution. One drawback of the deconvolution process is the amplification of the noise, since the latter acts on small image scales which belong to the high spatial frequency range. Therefore the deconvolution, which aims at enhancing the spatial resolution of the image, also amplifies the noise. For the restoration, we use the Richardson-Lucy (RL) algorithm.[18,19] The RL is an iterative algorithm, so the noise level (and consequently the RMS contrast of the reconstructed image) increases by increasing the number of iterations. In Figure 4 we show this effect by plotting the factor by which the noise increases after reconstruction (left panel) and the RMS contrast of the reconstructed image (right panel) as a function of the iteration number. We use the wavelet algorithm described in[20] to estimate the noise level in the continuum images. This method assumes that the noise is Gaussian only.

We also experimented with other filtering algorithms like the Wiener filtering technique. However, this method requires a proper choice of a regularisation parameter,[21] which in return affects the noise level and RMS contrast of the restored image as well. The restored images in Figure 5 correspond to an RL iteration number such that the noise level in the reconstructed data does not exceed 3.5 times the amount of noise in the unrestored data.

*https://github.com/fakahil/PyPD

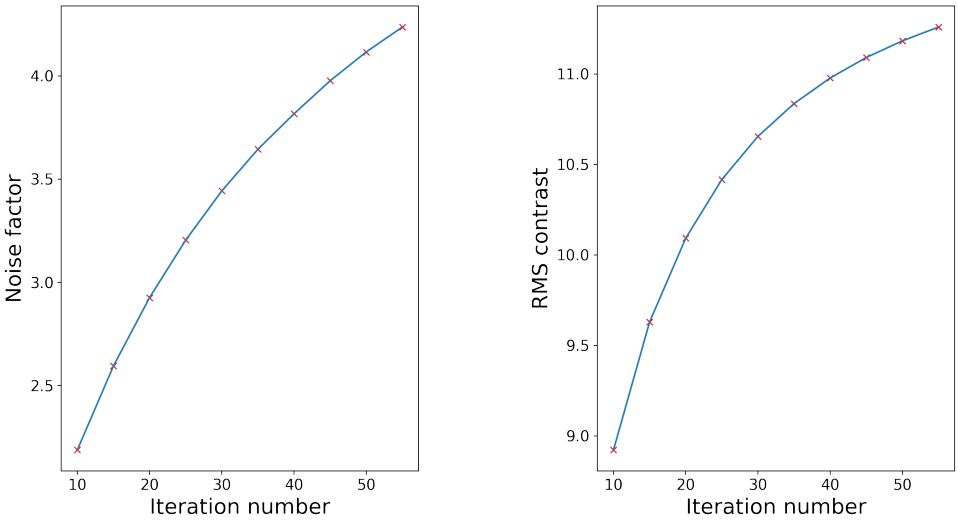

Figure 4. The ratio of the noise in the reconstructed image to that of the focused image (left panel), with 1 being the ratio in the focused image, and the RMS contrast of the reconstructed image (right panel) as a function of the iteration number of the RL filtering algorithm.

3. DISCUSSION AND CONCLUSIONS

We have characterised the optical aberrations in the optical path of SO/PHI-HRT on-board the Solar Orbiter spacecraft. We have reduced and analysed different calibration data adequate for image quality analysis. In particular, we have applied the powerful phase diversity technique to retrieve the wavefront aberrations, and therefore the PSF of the SO/PHI-HRT (Section 2). Our analysis confirms a common wavefront error over the field of view of the telescope, as expected from thermal lensing effects of the hot HREW, which is in the pupil of the PHI optical system, and which reaches temperatures of around 200 °C at perihelion conditions. We also studied the variation of the PSF in the image plane of SO/PHI-HRT under different thermal conditions (different distances to the Sun). We found that the wavefront quality decreases with decreasing distance of SO to the Sun, but thanks to the PD technique, the computed PSF ensures the restoration of the observed scene to have the same RMS contrast values at any distance from the Sun.

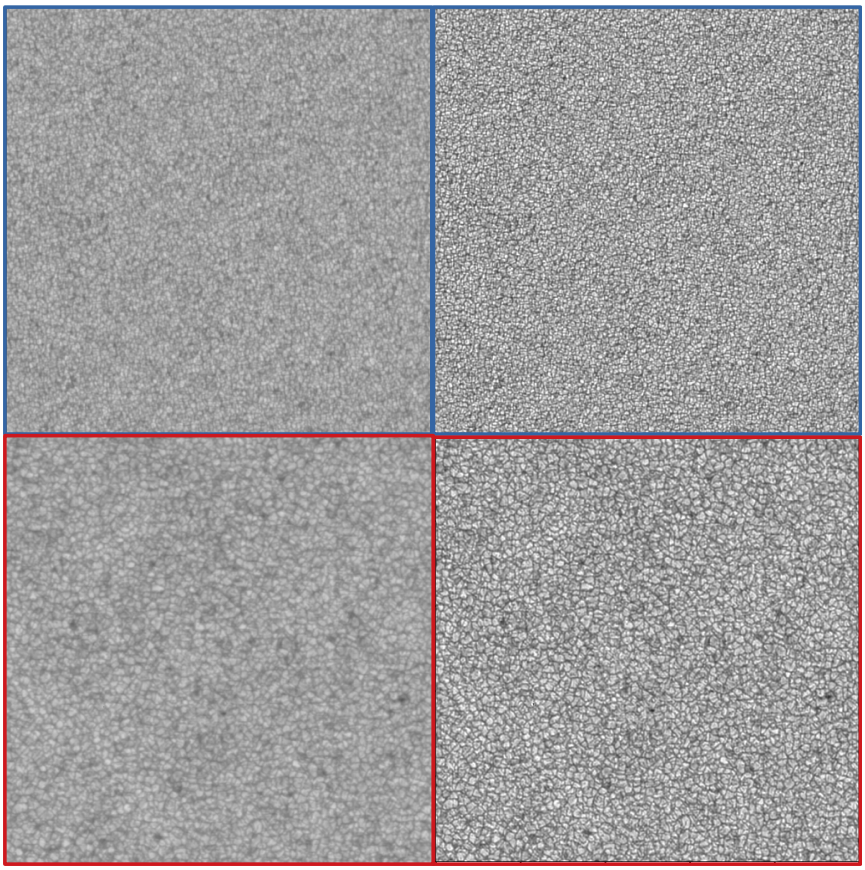

Figure 5. Raw (left column) and restored (right column) SO/PHI-HRT continuum images: The four panels show the central 500×500 pixels sub-region of the fully calibrated focused image of the PD image pair taken during PHI-5 at a distance of 0.82 AU from the Sun (top row) and during STP-136 at 0.523 AU (bottom row). Images are saturated within the range of 0.5−1.3 of the mean quiet-Sun intensity.

ACKNOWLEDGMENTS

Solar Orbiter is a space mission of international collaboration between ESA and NASA, operated by ESA. We are grateful to the ESA SOC and MOC teams for their support. The German contribution to SO/PHI is funded by the BMWi through DLR and by MPG central funds. The Spanish contribution is funded by FEDER/AEI/MCIU (RTI2018-096886-C5), a "Center of Excellence Severo Ochoa" award to IAA-CSIC (SEV-2017-0709), and a Ramón y Cajal fellowship awarded to DOS. The French contribution is funded by CNES.

REFERENCES

[1] Müller, D., St. Cyr, O. C., Zouganelis, I., Gilbert, H. R., Marsden, R., Nieves-Chinchilla, T., Antonucci, E., Auchère, F., Berghmans, D., Horbury, T. S., Howard, R. A., Krucker, S., Maksimovic, M., Owen, C. J., Rochus, P., Rodriguez-Pacheco, J., Romoli, M., Solanki, S. K., Bruno, R., Carlsson, M., Fludra, A., Harra, L., Hassler, D. M., Livi, S., Louarn, P., Peter, H., Schühle, U., Teriaca, L., del Toro Iniesta, J. C., Wimmer-Schweingruber, R. F., Marsch, E., Velli, M., De Groof, A., Walsh, A., and Williams, D., "The Solar Orbiter mission: Science overview," *A&A* **642**, A1 (Oct. 2020).

[2] Solanki, S. K., del Toro Iniesta, J. C., Woch, J., Gandorfer, A., Hirzberger, J., Alvarez-Herrero, A., Appourchaux, T., Martínez Pillet, V., Pérez-Grande, I., Sanchis Kilders, E., Schmidt, W., Gómez Cama, J. M., Michalik, H., Deutsch, W., Fernandez-Rico, G., Grauf, B., Gizon, L., Heerlein, K., Kolleck, M., Lagg, A., Meller, R., Müller, R., Schühle, U., Staub, J., Albert, K., Alvarez Copano, M., Beckmann, U., Bischoff, J., Busse, D., Enge, R., Frahm, S., Germerott, D., Guerrero, L., Löptien, B., Meierdierks, T., Oberdorfer, D., Papagiannaki, I., Ramanath, S., Schou, J., Werner, S., Yang, D., Zerr, A., Bergmann, M., Bochmann, J., Heinrichs, J., Meyer, S., Monecke, M., Müller, M.-F., Sperling, M., Álvarez García, D., Aparicio, B., Balaguer Jiménez, M., Bellot Rubio, L. R., Cobos Carracosa, J. P., Girela, F., Hernández Expósito, D., Herranz, M., Labrousse, P., López Jiménez, A., Orozco Suárez, D., Ramos, J. L., Barandiarán, J., Bastide, L., Campuzano, C., Cebollero, M., Dávila, B., Fernández-Medina, A., García Parejo, P., Garranzo-García, D., Laguna, H., Martín, J. A., Navarro, R., Núñez Peral, A., Royo, M., Sánchez, A., Silva-López, M., Vera, I., Villanueva, J., Fourmond, J.-J., de Galarreta, C. R., Bouzit, M., Hervier, V., Le Clec'h, J. C., Szwec, N., Chaigneau, M., Buttice, V., Dominguez-Tagle, C., Philippon, A., Boumier, P., Le Cocguen, R., Baranjuk, G., Bell, A., Berkefeld, T., Baumgartner, J., Heidecke, F., Maue, T., Nakai, E., Scheiffelen, T., Sigwarth, M., Soltau, D., Volkmer, R., Blanco Rodríguez, J., Domingo, V., Ferreres Sabater, A., Gasent Blesa, J. L., Rodríguez Martínez, P., Osorno Caudel, D., Bosch, J., Casas, A., Carmona, M., Herms, A., Roma, D., Alonso, G., Gómez-Sanjuan, A., Piqueras, J., Torralbo, I., Fiethe, B., Guan, Y., Lange, T., Michel, H., Bonet, J. A., Fahmy, S., Müller, D., and Zouganelis, I., "The Polarimetric and Helioseismic Imager on Solar Orbiter," *A&A* **642**, A11 (Oct. 2020).

[3] Albert, K., Hirzberger, J., Kolleck, M., Jorge, N. A., Busse, D., Rodríguez, J. B., Carrascosa, J. P. C., Fiethe, B., Gandorfer, A., Germerott, D., Guan, Y., Guerrero, L., Gutierrez-Marques, P., Expósito, D. H., Lange, T., Michalik, H., Suárez, D. O., Schou, J., Solanki, S. K., Iniesta, J. C. d. T., and Woch, J., "Autonomous on-board data processing and instrument calibration software for the Polarimetric and Helioseismic Imager on-board the Solar Orbiter mission," *JATIS* **6** (Dec. 2020).

[4] Gandorfer, A., Grauf, B., Staub, J., Bischoff, J., Woch, J., Hirzberger, J., Solanki, S. K., Álvarez-Herrero, A., García Parejo, P., Schmidt, W., Volkmer, R., Appourchaux, T., and del Toro Iniesta, J. C., "The High Resolution Telescope (HRT) of the Polarimetric and Helioseismic Imager (PHI) onboard Solar Orbiter," in [*Space Telescopes and Instrumentation 2018: Optical, Infrared, and Millimeter Wave*], Lystrup, M., MacEwen, H. A., Fazio, G. G., Batalha, N., Siegler, N., and Tong, E. C., eds., *Society of Photo-Optical Instrumentation Engineers (SPIE) Conference Series* **10698**, 106984N (July 2018).

[5] Zouganelis, I., De Groof, A., and Walsh, e. a., "The Solar Orbiter Science Activity Plan: Translating solar and heliospheric physics questions into action," *A&A* **642**, A3 (Oct. 2020).

[6] Paxman, R. G. and Crippen, S. L., "Aberration correction for phased-array telescopes using phase diversity," 787–797 (Nov. 1990).

[7] Löfdahl, M. G. and Scharmer, G. B., "Wavefront sensing and image restoration from focused and defocused solar images.," *ApJS* **107**, 243–264 (Oct. 1994).

[8] Paxman, R. G., Thelen, B. J., and Seldin, J. H., "Phase-diversity correction of turbulence-induced space-variant blur," *Opt. Lett.* **19**, 1231 (Aug. 1994).

[9] Danilovic, S., Gandorfer, A., Lagg, A., Schüssler, M., Solanki, S. K., Vögler, A., Katsukawa, Y., and Tsuneta, S., "The intensity contrast of solar granulation: comparing Hinode SP results with MHD simulations," **484**, L17–L20 (June 2008).

[10] Noll, R. J., "Zernike polynomials and atmospheric turbulence*," *J. Opt. Soc. Am.* **66**, 207 (Mar. 1976).

[11] Lakshminarayanan, V. and Fleck, A., "Zernike polynomials: a guide," *Journal of Modern Optics* **58**, 545–561 (Apr. 2011).

[12] Gonsalves, R. A., "Fundamentals Of Wavefront Sensing By Phase Retrieval," 56–65 (Aug. 1983).
[13] Gonsalves, R. A., "Phase Retrieval," 202 (July 1985).
[14] Fried, D. L., "Post-Detection Wavefront Distortion Compensation," 127 (Jan. 1988).
[15] Danilovic, S., Gandorfer, A., Lagg, A., Schüssler, M., Solanki, S. K., Vögler, A., Katsukawa, Y., and Tsuneta, S., "The intensity contrast of solar granulation: comparing Hinode SP results with MHD simulations," *A&A* **484**, L17–L20 (June 2008).
[16] Riethmüller, T. L., Solanki, S. K., Berdyugina, S. V., Schüssler, M., Pillet, V. M., Feller, A., Gandorfer, A., and Hirzberger, J., "Comparison of solar photospheric bright points between Sunrise observations and MHD simulations," *A&A* **568**, A13 (Aug. 2014).
[17] Hirzberger, J., Feller, A., Riethmüller, T. L., Gandorfer, A., and Solanki, S. K., "Performance validation of phase diversity image reconstruction techniques," *A&A* **529**, A132 (May 2011).
[18] Richardson, W. H., "Bayesian-Based Iterative Method of Image Restoration," *Journal of the Optical Society of America (1917-1983)* **62** (Jan. 1972).
[19] Lucy, L. B., "An iterative technique for the rectification of observed distributions," *ApJ* **79** (June 1974).
[20] Donoho, D. L. and Johnstone, I. M., "Ideal spatial adaptation by wavelet shrinkage," *Biometrika* **81**, 425–455 (Sept. 1994).
[21] Van Noort, M., Der Voort, L. R. V., and Löfdahl, M. G., "Solar Image Restoration By Use Of Multi-frame Blind De-convolution With Multiple Objects And Phase Diversity," *Sol Phys* **228**, 191–215 (May 2005).